Journal of Energy & Environment

Journal homepage: journal.uniten.edu.my/jee

ISSN: 1985-7462

A Parametric Optimization using Taguchi Method for Cu(In,Ga)(S,Se)$_2$ Thin Film Solar Cell Device Simulation

M. S. Bahrudin[a] , Y. Yusoff[b], S. F. Abdullah[a], A. W. M. Zuhdi[b], N. Amin[b] and I. Ahmad[b]

[a] College of Engineering, Universiti Tenaga Nasional, 43000 Kajang, Malaysia.
[b] Institute of Sustainable Energy, Universiti Tenaga Nasional, 43000 Kajang, Malaysia.

Keywords

CIGS
solar cell
double grading
Taguchi

Abstract

In this simulation study, Taguchi Method was used to investigate the influence of the absorber layer grading profile on the photovoltaic performance of CIGS solar cells. The work is simulation-based whereby the solar cell model was created and simulated using SCAPS-1d software. Four control factors have been chosen, such as the band gap minimum ($E_{g,min}$), the position of the band gap minimum ($X_{Eg,min}$), the band gap of the absorber layer towards the buffer layer ($E_{g,front}$), and the band gap of the absorber towards the back contact ($E_{g,rear}$). The aim is to find the most suitable combination of control factors that result in the most favorable outcomes for open circuit voltage (V_{oc}), short circuit current density (J_{sc}) and fill factor (FF) over acceptor concentration ranging from 2.0×10^{14} to 2.0×10^{16} cm^{-3} and donor concentration between 1.0×10^{17} to 1.0×10^{19} cm^{-3}. The results show that the highest power conversion efficiency was achieved using a combination of high-level $E_{g,min}$ with low-level $X_{Eg,min}$, middle-level $E_{g,front}$ and high-level $E_{g,rear}$. The simulated device demonstrated an average efficiency of 22.08% with corresponding J_{sc} = 43.05 mA/cm^2, V_{oc} = 0.704 V and FF = 76.37. Confirmation test on the developed model from Taguchi Method demonstrates a robust characteristics on all outcomes against the realistic carrier concentration range mentioned above.

1. INTRODUCTION

The band gap of the quinary Cu(In,Ga)(Se,S)$_2$ compound semiconductor can be changed by varying the composition of gallium (Ga) to indium (In) ratio and sulfur (S) to selenium (Se) ratio in the film. This property makes it possible to tailor the band gap of the absorber layer throughout its entire thickness resulting in an absorber layer with a graded bandgap profile. According to Decock et al. in [1] and [2], two effects come into play with bandgap grading. Increasing the band gap at one part helps to reduce recombination in that part of the cell. However, it also deteriorates the photon absorption rate. Secondly, changing the band level will cause additional electric fields to be generated within the cell. Thus, two simultaneous approaches are commonly used in the fabrication of high efficiency CIGS devices. These are, increasing the band gap towards the buffer-absorber interface, also known as front grading, and increasing the band gap towards the back contact, also known as back grading. However, both profiles are not without their limitations. Front grading introduces a counteracting electric field and shifts the absorption region away from the space charge region (SCR) and lead to large losses on short circuit current (J_{sc}) and fill factor (FF) [3]. Meanwhile, back grading increases the band gap in the region closest to the back contact while the front surface remains lower in bandgap energy. This configuration has the negative impact of restricts the absorption of high energy photons in the absorber layer. Combining the two approaches produces an absorber layer with double band gap grading profile. Devices with double graded absorber layers have been shown to have better performance with improved open circuit voltage (V_{oc}) and enhanced collection of photogenerated carriers [4]. Therefore, double graded bandgap absorbers are now considered a necessary feature of high efficiency CIGS photovoltaic devices. However, the parameters of bandgap points need to be optimized to maximize the device's power conversion efficiency.

Although numerous simulation attempts have been made, these were mainly based on the trial and error method of optimization. The optimization attempts can be simplified with the usage of the Taguchi Optimization Method (Taguchi method) [5]. Taguchi method has been widely used for improving productivity during research and devel-

opment. It is implemented as an orthogonal array to study the bandgap points to find the best values that could balance the outputs. This, in other words, can minimize the number of parameters that are to be used in device simulation, thereby saving cost and time [6].

2. EXPERIMENTAL DETAILS

A reference case was first developed based on the complete structure of CIGS solar cell made by Solar Frontier, as shown in Figure 1(a) [7]. The device's power conversion simulation studies were performed using Solar Cell Capacitance Simulator (SCAPS-1d) software version 3.3.08 developed at the University of Gent, Belgium [8]. The solar cell structure is simulated following the configuration of ZBO/ZnMgO/ZnS/CIGSSe. Usually, in high efficiency CIGS devices, the absorber layer has a thickness ranging from 2 to 2.3 μm [2]. However, for this study thickness of the CIGSSe absorber layer is fixed to 2 μm considering the most recent works of literature' experimental data [9] [10] [11].

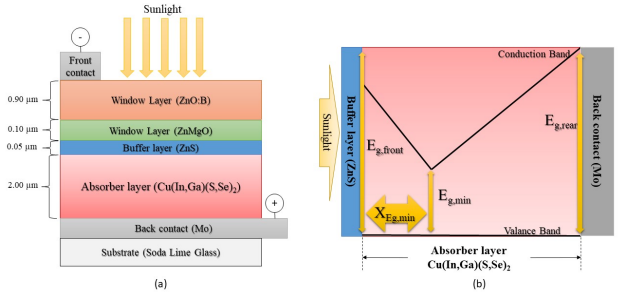

Figure 1. (a) Full device structure, (b) Parameters of interest inside the absorber layer

There are four parameters of interest as shown in Figure 1(b). The first three are the three bandgap points: the front bandgap ($E_{g,front}$) that is located at the absorber region close to the buffer layer, the minimum bandgap ($E_{g,min}$) located within the bulk area of the absorber, and the rear bandgap ($E_{g,rear}$) located in the absorber region close to the back contact. While $E_{g,front}$ and $E_{g,rear}$ locations are shifted only along the y-axis, the $E_{g,min}$ is also shifted along the x-axis represented by $X_{Eg,min}$ as the fourth parameter.

Electrical characteristics with relevant parameters and are as listed in Table 1. These parameters are chosen based on existing experimental data, literature review as well as by reasonable estimation based on theoretical considerations [12]–[15].

Parameters that are listed as 'varied' are the parameters of interest used for Taguchi Optimization. It is noted that the value of electron affinity X_e changes with E_g [11].

Table 1. Parameters of relevant layers of the CIGS solar cell

Parameters	ZBO	ZnMgO	ZnS	CIGSSe
E_g (eV)	3.6	3.65	3.72	Varied
X_e (eV)	4.6	4.6	4.6	Varied
N_c (cm^{-3})	2.2×10^{18}	2.2×10^{18}	2.2×10^{18}	2.2×10^{18}
N_v (cm^{-3})	1.8×10^{19}	1.8×10^{19}	1.8×10^{19}	1.8×10^{19}
V_{eth} (cm/s)	1.0×10^{8}	1.0×10^{7}	1.0×10^{7}	1.0×10^{7}
V_{pth} (cm/s)	1.0×10^{8}	1.0×10^{7}	1.0×10^{7}	1.0×10^{7}
U_e (cm2/Vs)	1.0×10^{2}	1.0×10^{2}	1.0×10^{2}	1.0×10^{2}
U_p (cm2/Vs)	3.1×10^{1}	2.5×10^{1}	2.5×10^{1}	$2.5x10^{1}$
N_D (cm^{-3})	1.0×10^{18}	1.0×10^{17}	Varied	-
N_A (cm^{-3})	-	-	-	Varied

3. TAGUCHI METHOD WITH ORTHOGONAL ARRAY L9

The four parameters mentioned in the previous section are defined as control factors. Table 2 shows these control factors with their respected levels. Taguchi method requires three levels such as the lowest, the middle and the high values.

Table 2. Control factors and their respective levels

Control factors	Unit	Levels 1	2	3
$X_{Eg,min}$	μm	0.10	0.20	0.30
$E_{g,min}$	eV	1.06	1.08	1.1
$E_{g,front}$	eV	1.20	1.47	1.76
$E_{g,rear}$	eV	1.30	1.44	1.59

The level variation for $X_{Eg,min}$ are taken based on Kato et al. in [7] that stated $X_{Eg,min}$ should be below 0.3 μm from the buffer layer. $E_{g,min}$, $E_{g,front}$ and $E_{g,rear}$ was calculated using formula (1)

$$E_g^{CIGSSe}(X,Y) = (1.00 + 0.13X^2 + 0.08X^2Y + 0.13XY + 0.55X + 0.54Y)eV \quad (1)$$

Where X is the composition ratio of [Ga]/[Ga+In] and Y is the composition ratio of [S]/[S + Se]. Using equation (1), it is possible to determine variation of Cu(In,Ga)(S,Se)^2 bandgap for any given set of $0 \leq X \leq 1$ and $0 \leq Y \leq 1$ values [16].

Acceptor concentration (N_A) and donor concentration (N_D) listed in Table 3 are designated as the noise factor. These factors are considered uncontrollable because during the fabrication of the CIGS layer, no doping process involved. The values of N_A and N_D depended solely on the defects present in the absorber layer. The values listed in Table 3 is the typical concentration ranges found in works of literature [11], [12], [15], [17].

Table 4 shows the orthogonal array that is used as the experimental layout where all respective control factors' level was arranged as indicated. For this study, the Taguchi

Table 3. Noise factors and their respective level

Noise factors	Unit	Noise levels		
		1	2	3
N_A	cm^{-3}	2.0×10^{14}	2.0×10^{15}	2.0×10^{16}
N_D	cm^{-3}	1.0×10^{17}	1.0×10^{18}	1.0×10^{19}

method involved an L9 orthogonal array (L9) with nine iterations of experiments [18]. L9 was chosen because it can handle up to four maximum control factors that are suitable for this study.

Table 4. Experimental layout of L9 orthogonal array

Expt. No.	Control factor and level			
	$X_{Eg,min}$	$E_{g,min}$	$E_{g,front}$	Backside E_g
1	1	1	1	1
2	1	2	2	2
3	1	3	3	3
4	2	1	2	3
5	2	2	3	1
6	2	3	1	2
7	3	1	3	2
8	3	2	1	3
9	3	3	2	1

Table 5 is the arrangement on the noise factor. Two noise factors with three levels each are equivalent to nine combinations of repetitions.

Table 5. Noise factor combinations with nine repetition

Repetition	Noise factor and level	
	N_A	N_D
1	1	1
2	2	2
3	3	3
4	1	2
5	2	3
6	3	1
7	1	3
8	2	1
9	3	2

These nine sets of experimental parameters and their respective repetitions were then simulated using SCAPS-1d software. The results of these iterations were divided into three outcomes, open circuit voltage (V_{oc}), short circuit current (J_{sc}) and fill factor (FF). These three outcomes are vital to calculate the efficiency of the solar cell using the expression:

$$\eta = \frac{V_{oc}\times J_{sc}\times FF}{P_{in}}(\%) \tag{2}$$

where η is the efficiency and P_{in} is the input power of 100 mW/cm^2 [19].

4. RESULTS AND DISCUSSION

Using electrical parameters and Taguchi parameters (in the form of L9 ortogonal array) listed on previous section, simulation on the CIGS solar cell is run using SCAPS-1d. The simulation results of the respective outcomes are shown in Tables 6, 7 and 8.

Based on these simulation results, the factors that substantially impacted the result can be determined. The first step is to convert the data from the results into signal-to-noise (S/N) ratio in order to signify their performance. There are three categories of S/N performance characteristics, lower-the-best, nominal-the-best and larger-the-best [20]. In this study, a larger-the-best S/N ratio was chosen because it aims to achieve maximum values for all the three outcomes. The S/N performance for larger-the-best is expressed as the following.

$$\eta = -10\log_{10}\left[\frac{1}{n}\sum(Y_1^{-2}+Y_2^{-2}+Y_3^{-2}+\ldots+Y_n^{-2})\right](dB) \tag{3}$$

Where n is the number of simulation and Y_n the simulation value of the V_{oc}, J_{sc} and FF (respectively). By applying expression (2), S/N ratio is summarized in Table 9.

The S/N ratio for each level on each control factor and their respective overall mean are summarized in Tables 10, 11 and 12.

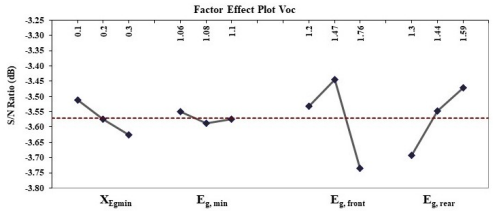

Figure 2. Factor effect plot for V_{oc}

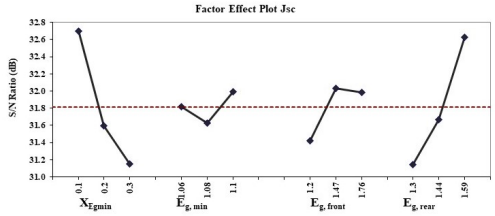

Figure 3. Factor effect plot for J_{sc}

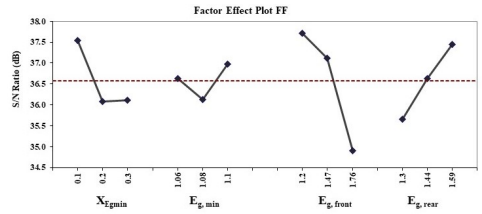

Figure 4. Factor effect plot for FF

Figures 2, 3 and 4 show the S/N ratio graphs. The dashed line on these graphs represents the overall mean value of the

Table 6. Simulation results on Open Circuit Voltage, V_{oc}

Expt. No.	Repetitions (V)								
	1	**2**	**3**	**4**	**5**	**6**	**7**	**8**	**9**
1	0.642	0.651	0.680	0.645	0.650	0.681	0.704	0.640	0.680
2	0.650	0.668	0.719	0.653	0.660	0.711	0.720	0.644	0.689
3	0.638	0.661	0.713	0.637	0.657	0.709	0.644	0.635	0.683
4	0.651	0.676	0.730	0.653	0.662	0.714	0.737	0.645	0.690
5	0.602	0.619	0.668	0.617	0.635	0.687	0.655	0.624	0.669
6	0.644	0.656	0.691	0.645	0.652	0.690	0.720	0.640	0.681
7	0.613	0.637	0.690	0.624	0.642	0.694	0.664	0.626	0.671
8	0.645	0.657	0.692	0.646	0.652	0.690	0.721	0.640	0.681
9	0.631	0.661	0.697	0.631	0.648	0.698	0.675	0.629	0.674

Table 7. Simulation results on Short Circuit Current, J_{sc} mA/cm^2

Expt. No.	Repetitions (mA/cm^2)								
	1	**2**	**3**	**4**	**5**	**6**	**7**	**8**	**9**
1	38.23	36.13	36.84	39.24	38.28	37.85	39.31	39.25	38.96
2	43.42	39.41	38.31	44.54	43.47	42.44	44.61	44.56	44.25
3	50.25	48.15	46.68	50.44	49.35	48.32	50.44	50.45	50.13
4	43.66	39.49	38.03	44.93	43.86	42.85	45.00	44.95	44.63
5	44.10	40.77	39.12	41.57	43.13	42.53	26.90	28.34	28.58
6	36.54	33.95	34.77	37.66	36.69	36.22	37.74	37.68	37.38
7	45.37	41.65	40.00	44.10	44.53	43.91	27.86	29.07	29.22
8	37.21	34.59	35.41	38.33	37.36	36.89	38.41	38.35	38.06
9	40.77	36.63	35.19	41.62	40.80	39.87	29.09	30.07	30.14

Table 8. Simulation result on FF

Expt. No.	Repetitions								
	1	**2**	**3**	**4**	**5**	**6**	**7**	**8**	**9**
1	76.88	78.70	80.25	77.44	77.21	79.21	72.29	79.28	79.73
2	77.12	77.21	79.13	77.13	76.20	76.24	69.17	78.84	79.30
3	76.94	78.68	79.58	76.05	78.05	78.51	52.13	70.04	73.43
4	75.15	72.76	73.85	77.14	76.13	75.96	69.61	79.32	79.64
5	34.36	42.57	47.44	41.63	39.86	39.24	57.90	64.30	64.19
6	73.55	75.27	78.81	77.31	76.61	78.58	70.70	79.30	79.70
7	51.09	56.65	59.69	46.39	45.17	44.44	60.43	66.80	66.69
8	73.37	75.00	78.70	77.30	76.65	78.60	70.59	79.31	79.73
9	69.79	67.26	68.73	57.34	58.06	58.29	63.09	69.57	69.42

Table 9. Summary of S/N ratio for all outcome

Exp No.	S/N Ratio (Larger-the-Better) (dB)		
	V_{oc}	J_{sc}	FF
1	-3.58	31.64	37.82
2	-3.38	32.59	37.68
3	-3.58	33.86	37.12
4	-3.33	32.63	37.54
5	-3.88	30.92	33.03
6	-3.52	31.23	37.67
7	-3.75	31.17	34.55
8	-3.51	31.39	37.66
9	-3.62	30.88	36.12

S/N ratio. The factor effect plots provide a clear view of how each control factor influences the outcomes' performance. Fundamentally, the level with the highest S/N ratio shown on the plot has the most influence on the outcomes and vice versa. However, the closer the plot is to the overall mean, the level (and the control factor) is negligible to the outcome's performance.

Table 10. (S/N) Ratio responses on each level and the overall mean for V_{oc}

Control factor parameters	S/N ratio (dB)			Overall Mean
	Level 1	**Level 2**	**Level 3**	
$X_{Eg,min}$	-3.51	-3.57	-3.63	-3.57
$E_{g,min}$	-3.55	-3.59	-3.57	
$E_{g,front}$	-3.53	-3.44	-3.74	
Backside E_g	-3.69	-3.55	-3.47	

$X_{Eg,min}$ shows a dominating effect on Jsc on the low-level value and in agreement with Kato et al stated that shallower $X_{Eg,min}$ ensure the $E_{g,min}$ is within the space charge region. [7]. All Factor effect plots for $E_{g,min}$ are shown closer to the overall mean line but relatively giving better S/N ratio at a high level on J_{sc} and FF. $E_{g,front}$ shows inconsistent results between V_{oc} and FF where middle level gave a better performance to V_{oc} and the low level is preferable for better FF performance. A low level, however, indicates poor performance for the J_{sc}. The best selection for $E_{g,front}$

Table 11. (S/N) Ratio responses on each level and the overall mean for J_{sc}

Control factor parameters	S/N ratio (dB) Level 1	Level 2	Level 3	Overall Mean
$X_{Eg,min}$	32.69	31.59	31.15	31.81
$E_{g,min}$	31.82	31.63	31.99	
$E_{g,front}$	31.42	32.03	31.98	
$E_{g,rear}$	31.14	31.66	32.63	

Table 12. (S/N) Ratio responses on each level and the overall mean for FF

Control factor parameters	S/N ratio (dB) Level 1	Level 2	Level 3	Overall Mean
$X_{Eg,min}$	37.54	36.08	36.11	36.58
$E_{g,min}$	36.63	36.12	36.97	
$E_{g,front}$	37.72	37.11	34.90	
$E_{g,rear}$	35.66	36.63	37.44	

is determined using Analysis of Variance in the next section. $E_{g,rear}$ shows significant performance on all outcomes, particularly the J_{sc}. This backed by the fact that bandgap increase toward the back of the absorber layer reduce recombination, increase carrier collection and increase the J_{sc} [21] [22].

A. Analysis of Variance (ANOVA)

It has been noted that there is an apparent disparity between the three factor effect plots. The factor effect plot for the $E_{g,front}$ indicates a contradictory performance where middle level produced better performance on V_{oc} but having a low-level value give the most on the FF. For this reason, a decomposition of variance called analysis of variance (ANOVA) is done for a better selection process [23]. Results on ANOVA are listed in Table 13.

From ANOVA results, it was found that the $E_{g,front}$ factor effect for V_{oc} has a slightly higher percentage than the $E_{g,front}$ factor effect for FF by 0.34%. Even though $E_{g,front}$ performance effect on Jsc is almost negligible, looking at the J_{sc} factor effect plot, level 2 shows the highest S/N ratio. Thus, level 2 value ($E_{g,front}$ = 1.47 eV) is considered for best level selection. Other control factors selection is pretty much direct. $X_{Eg,min}$ on level 1 and $E_{g,rear}$ on level 3 show the highest factor effect percentage on J_{sc} (46.86% and 42.48%, respectively). From the factor effect plot, shallower $X_{Eg,min}$ (i.e. $X_{Eg,min}$ = 0.1 µm) and higher $E_{g,rear}$ (i.e. $E_{g,rear}$ = 1.59 eV) give the best performance on all outcomes. The $E_{g,min}$ shows the strongest influence on the FF at 4.54%.

B. Confirmation Test

From factor effects plots and ANOVA, each control factor's best level is selected and finalized in Table 14. As a final step, a confirmation simulation is performed using the selected levels. The purpose of this simulation is to validate the conclusion drawn from the analysis. The confirmation test also includes the efficiency expressed by equation (2).

Table 13. Result on Anova for all outcome

Outcome	Control Factors	Degrees of Freedom	Sum of Squares	Mean Square	Factor Effect (%)
V_{oc}	$X_{Eg,min}$	2	0.019	0.010	5.04
	$E_{g,min}$	2	0.002	0.001	0.34
	$E_{g,front}$	2	0.134	0.067	59.15
	$E_{g,rear}$	2	0.076	0.038	35.47
J_{sc}	$X_{Eg,min}$	2	3.802	1.901	46.86
	$E_{g,min}$	2	0.194	0.097	2.33
	$E_{g,front}$	2	0.695	0.347	8.33
	$E_{g,rear}$	2	3.395	1.698	42.48
FF	$X_{Eg,min}$	2	4.174	2.087	17.15
	$E_{g,min}$	2	1.099	0.549	4.54
	$E_{g,front}$	2	13.200	6.600	58.81
	$E_{g,rear}$	2	4.801	2.401	19.50

Table 14. The best setting of the selected level

Control Factors	Unit	Best selection	Level for the best selection
$X_{Eg,min}$	µm	0.1	1
$E_{g,min}$	eV	1.1	3
$E_{g,front}$	eV	1.47	2
$E_{g,rear}$	eV	1.59	3

The confirmation test result was compiled in Table 15, along with their respective noise factor combinations.

The result displays the power conversion efficiency range is consistently well over 21% despite lower acceptor and donor concentration. Maximum efficiency of beyond 24% is achievable when the concentrations are at the highest. On the other hand, the minimum efficiency of 22.67% can be expected for the lowest N_A and N_D combination. The average efficiency was shown to be 23.08%. The table also shows the relationship between Voc and Jsc, where the latter is higher when the former is low and vice versa. Therefore, optimization by Taguchi manages to balance between the two for optimum efficiency. As a result, Voc, Jsc and FF's average values are 0.704 V, 43.05 mA/cm^2 and 76.37, respectively.

5. CONCLUSION

In this study, the optimum solution for CIGS solar cell power conversion efficiency is predicted by using the Taguchi Method. Using this method, a better understanding of the simulated parameters that affect the CIGS solar cell performance has been demonstrated, resulting in further improvement. The result predicted by the Taguchi method produced an impressive solar cell conversion efficiency of 24.86% compared to the recent simulation result by [24] that predicted efficiency of 24.5%.

ACKNOWLEDGMENT

This study is supported by URND Sdn. Bhd. research grant (project code: U-TE-RD-18-01). The author would like to thank Associate Professor Dr. Fauziyah Binti Salehuddin

Table 15. Results on confirmation test with its respective noise factor combination

Repetition (N_A,N_d)	**Unit**	**1 (1,1)**	**2 (2,2)**	**3 (3,3)**	**4 (1,2)**	**5 (2,3)**	**6 (3,1)**	**7 (1,3)**	**8 (2,1)**	**9 (3,2)**
V_{oc}	V	0.685	0.678	0.725	0.699	0.672	0.718	0.797	0.662	0.701
J_{sc}	mA/cm^2	43.76	40.56	38.95	44.41	43.76	42.89	44.45	44.42	44.22
FF		75.65	76.97	78.77	74.67	77.32	76.81	67.23	79.72	80.21
Efficiency (calculated)	%	22.67	21.16	22.23	23.18	22.74	23.65	23.83	23.45	24.86

from Universiti Teknikal Melaka (UTeM) for her Taguchi Optimization Method expertise.

REFERENCES

[1] K. Decock, J. Lauwaert, and M. Burgelman, "Characterization of graded CIGS solar cells," *Energy Procedia*, vol. 2, no. 1, pp. 49–54, Aug. 2010. DOI: 10.1016/j.egypro.2010.07.009.

[2] K. Decock, J. Lawaert, and M. Burgelman, "Modelling thin film solar cells with graded band gap," in *45th International conference on Microelectronics devices and technologies (MIDEM 2009)*, MIDEM-Society for Microelectronics, Electronic Components and Materials, 2009, pp. 245–249.

[3] M. Gloeckler and J. Sites, "Band-gap grading in Cu(In,Ga)Se_2 solar cells," *Journal of Physics and Chemistry of Solids*, vol. 66, no. 11, pp. 1891–1894, Nov. 2005. DOI: 10.1016/j.jpcs.2005.09.087.

[4] A. Parisi, R. Pernice, V. Rocca, L. Curcio, S. Stivala, A. C. Cino, G. Cipriani, V. D. Dio, G. R. Galluzzo, R. Miceli, and A. C. Busacca, "Graded carrier concentration absorber profile for high efficiency CIGS solar cells," *International Journal of Photoenergy*, vol. 2015, pp. 1–9, 2015. DOI: 10.1155/2015/410549.

[5] S. B. Patel and J. V. Gohel, "Enhanced solar cell performance by optimization of spray coated CZTS thin film using Taguchi and response surface method," *Journal of Materials Science: Materials in Electronics*, vol. 29, no. 7, pp. 5613–5623, Jan. 2018. DOI: 10.1007/s10854-018-8530-5.

[6] G. Taguchi, *The System of Experimental Design: Engineering Methods to Optimize Quality and Minimize Costs*. 1987.

[7] T. Kato, "Cu(In,Ga)(Se,S)$_2$ solar cell research in Solar Frontier: Progress and current status," *Japanese Journal of Applied Physics*, vol. 56, no. 4S, 04CA02, Feb. 2017. DOI: 10.7567/jjap.56.04ca02.

[8] M. Burgelman, K. Decock, A. Niemegeers, J. Verschraegen, and S. Degrave, "SCAPS manual," *February*, 2016.

[9] T. Kobayashi, H. Yamaguchi, Z. J. L. Kao, H. Sugimoto, T. Kato, H. Hakuma, and T. Nakada, "Impacts of surface sulfurization on Cu($In_1 - x$,Ga_x)Se_2 thin-film solar cells," *Progress in Photovoltaics: Research and Applications*, vol. 23, no. 10, pp. 1367–1374, Oct. 2014. DOI: 10.1002/pip.2554.

[10] K. F. Tai, R. Kamada, T. Yagioka, T. Kato, and H. Sugimoto, "From 20.9 to 22.3% Cu(In,Ga)(S,Se)$_2$ solar cell: Reduced recombination rate at the heterojunction and the depletion region due to K-treatment," *Japanese Journal of Applied Physics*, vol. 56, no. 8S2, p. 08MC03, Jul. 2017. DOI: 10.7567/jjap.56.08mc03.

[11] M. Saadat, M. Moradi, and M. Zahedifar, "CIGS absorber layer with double grading Ga profile for highly efficient solar cells," *Superlattices and Microstructures*, vol. 92, pp. 303–307, Apr. 2016. DOI: 10.1016/j.spmi.2016.02.036.

[12] A. Bauer, S. Sharbati, and M. Powalla, "Systematic survey of suitable buffer and high resistive window layer materials in $CuIn_{1-x}$ Ga_x Se_2 solar cells by numerical simulations," *Solar Energy Materials and Solar Cells*, vol. 165, pp. 119–127, Jun. 2017. DOI: 10.1016/j.solmat.2016.12.035.

[13] T. Kobayashi, Z. J. L. Kao, T. Kato, H. Sugimoto, and T. Nakada, "A comparative study of Cd- and Zn-compound buffer layers on Cu(In_{1-x},Ga_x)(S_y,Se_{1-y})$_2$ thin film solar cells," *Progress in Photovoltaics: Research and Applications*, vol. 24, no. 3, pp. 389–396, Oct. 2015. DOI: 10.1002/pip.2695.

[14] T. Nakada, "Invited paper: CIGS-based thin film solar cells and modules: Unique material properties," *Electronic Materials Letters*, vol. 8, no. 2, pp. 179–185, Apr. 2012. DOI: 10.1007/s13391-012-2034-x.

[15] M. Murata, D. Hironiwa, N. Ashida, J. Chantana, K. Aoyagi, N. Kataoka, and T. Minemoto, "Optimum bandgap profile analysis of Cu(In,Ga)Se_2 solar cells with various defect densities by SCAPS," *Japanese Journal of Applied Physics*, vol. 53, no. 4S, 04ER14, Jan. 2014. DOI: 10.7567/jjap.53.04er14.

[16] M. Bär, W. Bohne, J. Röhrich, E. Strub, S. Lindner, M. C. Lux-Steiner, C.-H. Fischer, T. P. Niesen, and F. Karg, "Determination of the band gap depth profile of the penternary Cu($In_{(1-X)}Ga_X$)($S_Y Se_{(1-Y)}$)$_2$ chalcopyrite from its composition gradient," *Journal*

of Applied Physics, vol. 96, no. 7, pp. 3857–3860, Oct. 2004. DOI: 10.1063/1.1786340.

[17] P. Chelvanathan, M. I. Hossain, and N. Amin, "Performance analysis of copper–indium–gallium–diselenide (CIGS) solar cells with various buffer layers by SCAPS," *Current Applied Physics*, vol. 10, no. 3, S387–S391, May 2010. DOI: 10.1016/j.cap.2010.02.018.

[18] M. S. Phadke, *Quality Engineering Using Robust Design*. Pearson Education, 2008.

[19] M. A. Green, "Solar cells: Operating principles, technology, and system applications," *Englewood Cliffs*, 1982.

[20] M. S. Bahrudin, S. F. Abdullah, I. Ahmad, A. W. M. Zuhdi, A. H. Hasani, F. Za'abar, M. Malik, and M. N. Harif, "J_{sc} and V_{oc} optimization of perovskite solar cell with interface defect layer using Taguchi method," in *2018 IEEE International Conference on Semiconductor Electronics (ICSE)*, IEEE, Aug. 2018. DOI: 10.1109/smelec.2018.8481203.

[21] V. Garg, B. S. Sengar, and S. Mukherjee, "A review on sputtered chalcopyrite and kesterite thin film solar cell," 2018.

[22] J. Ramanujam and U. P. Singh, "Copper indium gallium selenide based solar cells–a review," *Energy & Environmental Science*, vol. 10, no. 6, pp. 1306–1319, 2017.

[23] F. Salehuddin, I. Ahmad, F. A. Hamid, A. Zaharim, H. A. Elgomati, B. Y. Majlis, and P. Apte, "Influence of HALO and source/drain implantation variations on threshold voltage in 45nm CMOS technology," *International Journal of Electronics, Computer and Communications Technologies*, vol. 2, no. 3, pp. 27–33, 2012.

[24] N. E. I. Boukortt and S. Patanè, "Single junction-based thin-film CIGS solar cells optimization with efficiencies approaching 24.5 %," *Optik*, vol. 218, p. 165 240, Sep. 2020. DOI: 10.1016/j.ijleo.2020.165240.